Design Optimization of a Low-Speed Single-Sided Linear Induction Motor for Improved Efficiency and Power Factor

Article *in* IEEE Transactions on Magnetics · March 2008

DOI: 10.1109/TMAG.2007.912646 · Source: IEEE Xplore

CITATIONS
94

READS
903

3 authors, including:

Arash Hassanpour Isfahani

48 PUBLICATIONS **1,063** CITATIONS

SEE PROFILE

Bashir Ebrahimi

AURA SYSTEMS

67 PUBLICATIONS **2,633** CITATIONS

SEE PROFILE

Design Optimization of a Low-Speed Single-Sided Linear Induction Motor for Improved Efficiency and Power Factor

A. Hassanpour Isfahani, B. M. Ebrahimi, and H. Lesani

School of Electrical and Computer Engineering, University of Tehran, Tehran, Iran

Although linear electrical motors (LMs) are increasingly used in industry to develop linear motion, they suffer from two major drawbacks: low efficiency and low power factor. These drawbacks cause high energy consumption and a rise in input current, and occupy transmission line capacity. We present a multiobjective optimization method to improve both efficiency and power factor, simultaneously. Our method uses an analytical model of the machine to calculate the efficiency and power factor. It allows us to investigate the effects of various motor specifications on the efficiency and the power factor. Motor parameters and dimensions can then be optimized by using a genetic algorithm in an appropriate objective function. The results show an enhancement in motor performance. We have used 2-D and 3-D time-stepping finite-element methods to evaluate the analytical results. A comparison of results validates our optimization method.

Index Terms—**Efficiency, finite-element method, linear induction motor, optimization, power factor.**

I. Introduction

LINEAR ELECTRICAL MOTORS (LMs) offer numerous advantages over rotary ones in linear motion developing, notably absence of mechanical gears and transmission systems, which results in higher efficiency, higher dynamic performance, and improved reliability [1]. Among various types of linear motors, the linear induction motor (LIM) especially attracts attention because of its simple structure and low cost [2], [3]. Different types of LIMs have been presented so far. Flat and tubular constructions are the most applicable topologies of LIMs. Some topologies of LIMs employ aluminum cages in their secondary [4]. However, the use of an aluminum sheet instead of aluminum cages makes LIMs' structure simpler.

Proper performance of LIMs requires optimization of their design and control. Design of LIMs differs from that of rotary induction motors in some aspects; therefore, a specific design algorithm should be devised for them. Design of LIMs has so far been presented based on different modeling techniques including magnetic equivalent circuit (MEC), layer model, and finite-element method (FEM) [5]–[7]. MEC has some advantages over other methods for preliminary design of LIMs which lie in its simplicity and suitability for optimization. Therefore, in this paper an appropriate MEC model is used for the design optimization.

Design optimization of LIMs has been considered in many researches so far in which different objectives have been studied. Reduction of the primary weight has been considered in [8]. T. Yokoi has presented a linear programming technique to maximize the developed force at specific velocity [9]. The noise generated by the LIM has been reduced by selecting proper material for the primary core [10]. M. Kitamura *et al.* have used the direct search method and the 2-D magnetic field model to reach the optimal shape of core and conductors in LIMs in order to maximize the developed thrust and power to weight ratio [11]. Optimum arrangement and design of winding have also been studied [12], [13]. The eigenvalue analysis method has been used to improve the thrust and speed characteristics of an LIM [14]. Starting thrust of a low-speed LIM has been maximized under constant input current [15]. Lab scale LIMs have also been developed [16], [17]. A computer-based program has been developed to design an LIM with minimum weight and material volume [18]. Multiobjective optimization of LIMs has been considered as well. Primary weight, cost of secondary, and output volt ampere have been optimized simultaneously using sequential quadratic programming (SQP) [19]. Multiobjective optimal design of a slit-type LIM has been investigated [20]. In that research, starting thrust and output power to input volt ampere ratio have been considered as optimization objectives.

Unfortunately, efficiency and power factor have not gained enough attention in previous researches, while low efficiency leads to more energy consumption and low power factor causes more occupation of transmission line capacity and nonoptimal use of inverter. Usually, improvement in one feature might have an adverse effect on the other one. Therefore, a compromise is needed between the efficiency and the power factor. In order to achieve this goal, a multiobjective optimization is employed in this paper. First, an analytical model is presented for LIMs. An effective objective function regarding the efficiency and the power factor is then proposed and the genetic algorithm is used to optimize design parameters. Finally, the 2-D and 3-D time-stepping nonlinear FEM is carried out to evaluate the design optimization.

II. MEC of Linear Induction Motor

The topology of the proposed LIM is depicted in Fig. 1. It consists of a three-phase primary and an aluminum sheet laid on the secondary back iron. A simple magnetic equivalent circuit (MEC) for LIMs is shown in Fig. 2. Parameters values of the circuit can be obtained as follows [3]:

$$X_m = \frac{12\mu_0\omega_l a_e k_w^2 \tau N_{\rm ph}^2}{\pi^2 p g_{\rm ei}} \tag{1}$$

$$X_1 = \frac{2\mu_0\omega_l}{p}\left[\left(\lambda_s\left(1+\frac{3}{2p}\right)+\lambda_d\right)\cdot\frac{2a}{q}+\lambda_e l_{\rm ce}\right]N_{\rm ph}^2 \tag{2}$$

$$R_1 = \frac{1}{\sigma_c}\left(\frac{4a+2l_{\rm ce}}{N_{\rm ph}I}\right)J_c N_{\rm ph}^2 \tag{3}$$

$$R_2' = \frac{12 a_e k_w^2 N_{\rm ph}^2}{\tau d p \sigma_{\rm ei}} \tag{4}$$

Digital Object Identifier 10.1109/TMAG.2007.912646

Color versions of one or more of the figures in this paper are available online at http://ieeexplore.ieee.org.

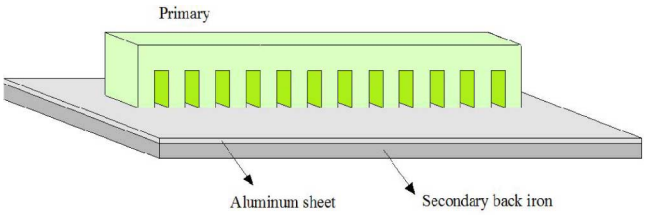

Fig. 1. Topology of a single-sided LIM.

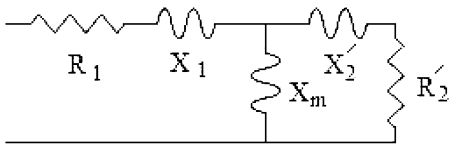

Fig. 2. Equivalent circuit of a LIM.

for the secondary sheet $X_2' \approx 0$. As it is seen in (1) and (4), saturation, air gap leakage, and skin effect are taken into account by modifying air gap length and conductivity of Al sheets [3].

Edge effect due to secondary overhang causes an increase in the secondary resistance and reduction in the magnetizing reactance which are explained in [3]. End effects are divided into static end effect and dynamic end effect. Static end effect is due to the open character of magnetic circuit in LIMs and is negligible when the number of poles is larger than six. The dynamic end effects are caused by the relative motion between the primary and the secondary. This effect is important in high-speed applications and can be ignored in low-speed LIMs.

The goodness factor, one of the most important indicators in design procedure, is then given by [3]

$$G = \frac{2f_l \mu_0 \sigma_{\rm ei} d\tau}{\pi g_{\rm ei}}. \tag{5}$$

Equivalent current sheet of primary windings, $J_{\rm m}$, is found from the following relationship:

$$J_m = \frac{\sqrt{2} m N_{\rm ph} I k_w}{p\tau}. \tag{6}$$

Therefore, the amplitude of first component of flux density in the air gap is found as follows [3]:

$$B_{g1} = \left| \frac{j\mu_0 J_m}{\pi \frac{g_m}{\tau}(1 + jsG)} \right|. \tag{7}$$

If we keep air gap flux density below 0.5 T, then the iron losses is negligible and the thrust, the efficiency, and the power factor are given by [3]

$$F_x = \frac{3I^2 R_2'}{2sf_l\tau \left[\left(\frac{1}{sG}\right)^2 + 1 \right]} \tag{8}$$

$$\eta = \frac{F_x 2\tau f_l (1-s)}{F_x 2\tau f_l + 3I^2 R_1} \tag{9}$$

$$\cos\varphi = \frac{F_x 2\tau f_l + 3I^2 R_1}{3VI}. \tag{10}$$

Symbol definitions appear in the Appendix.

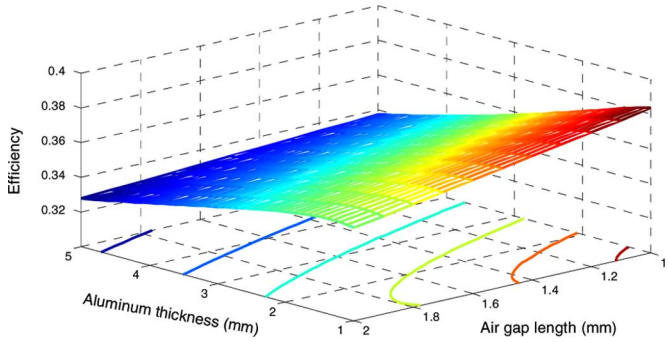

Fig. 3. Effects of air gap length and aluminum thickness on the efficiency of the analyzed LIM.

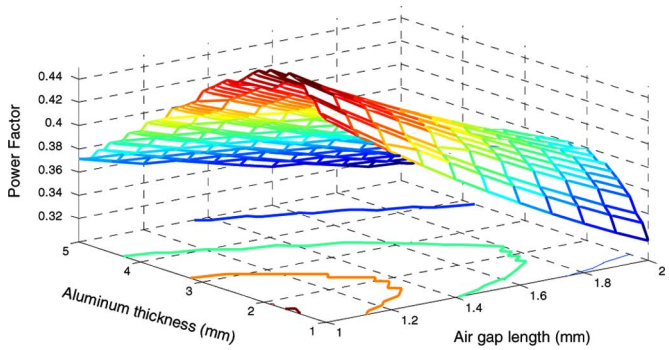

Fig. 4. Effects of air gap length and aluminum thickness on the power factor of the analyzed LIM.

III. Motor Analysis

In this section, variations of the efficiency and the power factor with design parameters are studied. Effects of the primary current density, the air gap length, the aluminum sheet thickness, the primary width to pole pitch ratio, the number of poles, the number of slots per pole per phase, and the maximum thrust slip are investigated.

Fig. 3 shows the variation of the efficiency with the air gap length and the aluminum thickness. It is seen that a reduction in the air gap length and the aluminum thickness leads to an increase in the efficiency. Fig. 4 shows the variations of the power factor with the air gap length and the aluminum thickness. It is seen that a reduction in the air gap length and the aluminum thickness leads to an increase in the power factor value. It is observed that the best aluminum thickness is between 1 and 2 mm. From the above results, we conclude that the air gap length should be selected as small as possible.

The variations of the efficiency and the power factor in terms of the maximum thrust slip and the primary width to pole pair ratio are shown in Figs. 5 and 6, respectively.

It is seen that the best efficiency is obtained at the slip value of 0.3; however, as the slip rises the power factor increases too.

It is also concluded that an increase in the primary width to pole pitch ratio leads to an increase in the power factor and a reduction in the efficiency.

Figs. 7 and 8 show the variations of the efficiency and the power factor with the number of pole pairs and the number of slots per pole per phase, respectively. It is seen that the number of pole pairs effectively affects the power factor; however, its effect on the efficiency is very small.

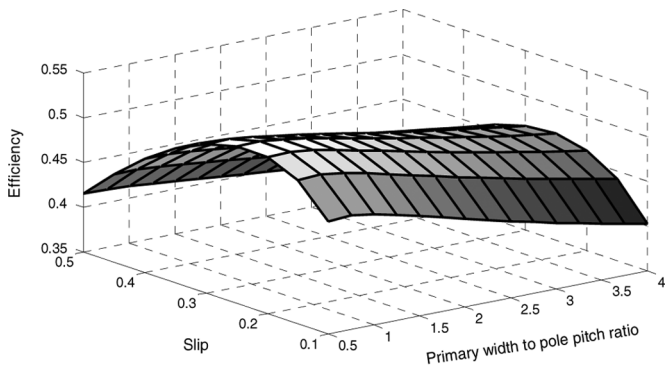

Fig. 5. Variation of the efficiency with the slip and the primary width to pole pitch ratio.

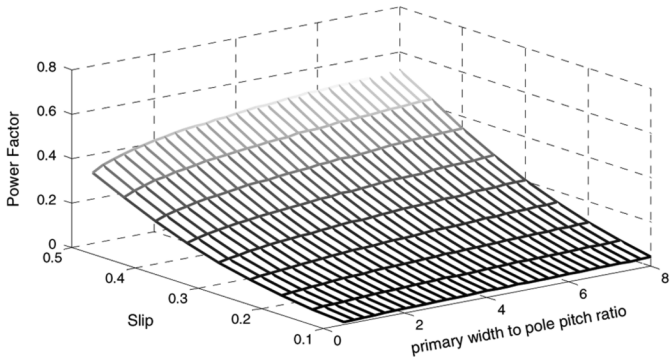

Fig. 6. Variation of the power factor with the slip and the primary width to pole pitch ratio.

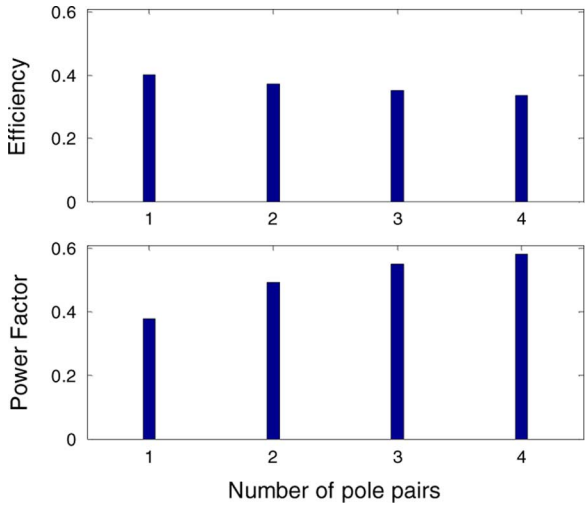

Fig. 7. Effects of the number of pole pairs on the efficiency and the power factor.

As the number of pole pairs increases, the efficiency decreases and the power factor increases. It is also seen that the number of slots per pole per phase does not have a considerable effect on efficiency but it may be influential on the power factor of LIMs. As the number of slots per pole per phase is increased, the power factor increases too.

Effects of primary current density on the power factor and the efficiency are depicted in Fig. 9. It is seen that higher current densities increase the power factor and reduce the efficiency of LIMs.

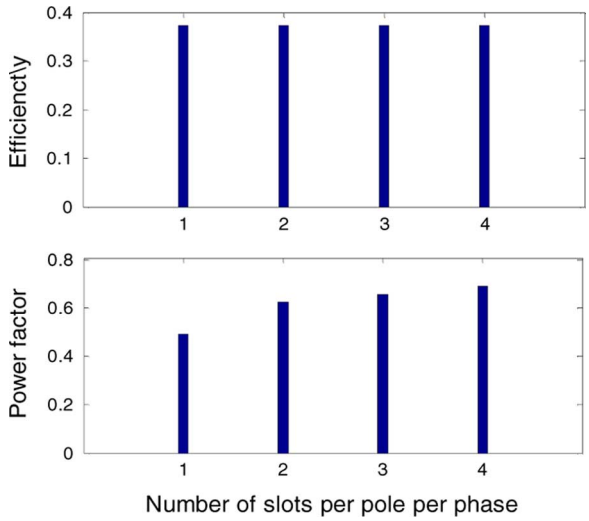

Fig. 8. Effects of the number of pole pairs on the efficiency and the power factor.

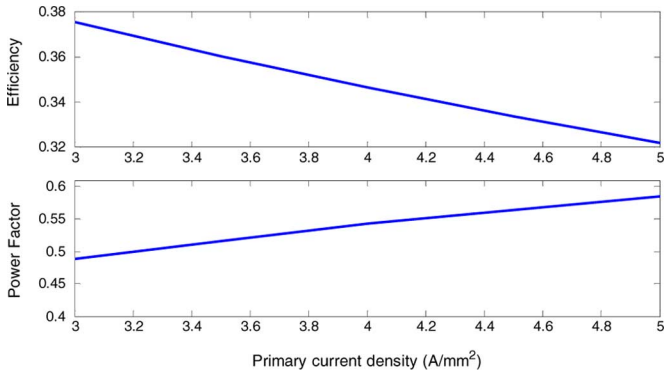

Fig. 9. Effects of the number of pole pairs on the efficiency and the power factor.

TABLE I
DESIGN CONSTRAINT

Parameter	Unit	Minimum Value	Maximum Value
Aluminum thickness	mm	1	4
Max. thrust slip	-	0.1	0.5
Primary current density	A/mm^2	3	5
Primary width / pole pitch	-	0.5	4
Efficiency	-	0.35	-
Power factor	-	0.3	-

It is observed that some of the design parameters have a different effect on the efficiency and the power factor and an increase in one of them may have an adverse effect on the other one. Thus, an optimization process is required to reach the optimal feasible design. In next sections, an optimization problem is defined and solved.

IV. Optimization Problem

Some of the typical LIM parameters and dimensions are selected as design variables whose values are determined through

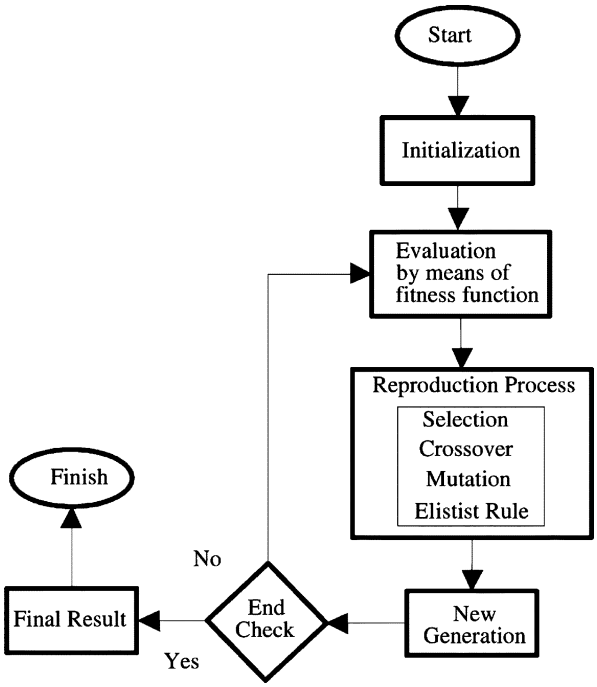

Fig. 10. Flowchart of genetic algorithm.

an optimization procedure. In this paper, design variables are the primary winding current density, the primary width to pole pitch ratio, the aluminum sheet thickness, and the maximum thrust slip. To have a more realistic design, some constraints are applied to design variables listed in Table I. The nominal thrust, the input voltage and frequency, and the mechanical velocity—the main fixed specifications in the design procedure—are 128 N, 220 V, 50 Hz, and 2.5 m/s, respectively.

The number of pole pairs and slots per pole per phase are chosen two and one, respectively. The simple one-layer winding is also used.

To obtain an optimal design considering both power factor and efficiency, the objective function is defined as follows:

$$J_\tau(x_1,\ldots,x_n) = \eta(x_1,\ldots,x_n)^{k_1} \cdot PF(x_1,\ldots,x_n)^{k_2} \quad (20)$$

where $x_1,\ldots,x_n$ are design variables. As seen in (20), the importance of the efficiency and the power factor are adjusted by power coefficients with regard to desirable performance. This importance can be supposed to be equal by using the same value for power coefficients. Maximization of J_τ fulfills simultaneously both objectives of the optimization. Such an objective function provides a higher degree of freedom in selecting appropriate design variables. A genetic algorithm is employed to search for maximum value of J_τ. The genetic algorithm provides a random search technique to find a global optimal solution in a complex multidimensional search space [21]. The algorithm consists of three basic operators, i.e., selection, crossover, and mutation. First, an initial population is produced randomly. Then, genetic operators are applied to the population to improve their fitness gradually. The procedure yields in new population at each iteration. Fig. 10 shows the flowchart of the genetic algorithm. In this paper, the Roulette wheel method is used for selection and at each step elite individual is sent directly to the next population. Table II shows genetic algorithm parameters used in this paper.

TABLE II
GENETIC ALGORITHM PARAMETERS

Parameter	Value
Probability of crossover	0.7
Probability of mutation	0.05
Population size	25
Number of Generations	150

TABLE III
SPECIFICATION OF INTIAL AND OPTIMAL DESIGNED MOTORS

Specification	Initial	Optimal 1	Optimal 2	Optimal 3
Efficiency	0.36	**0.393**	0.325	0.327
Power Factor	0.32	0.3	**0.42**	0.415
Obj. Func.	0.12	0.118	0.135	**0.135**
d (mm)	2	1.4	1.7	1.7
a/τ	2	2.5	3.9	3.9
s	0.5	0.5	0.5	0.5
J_c (A/mm^2)	4	3	5	5

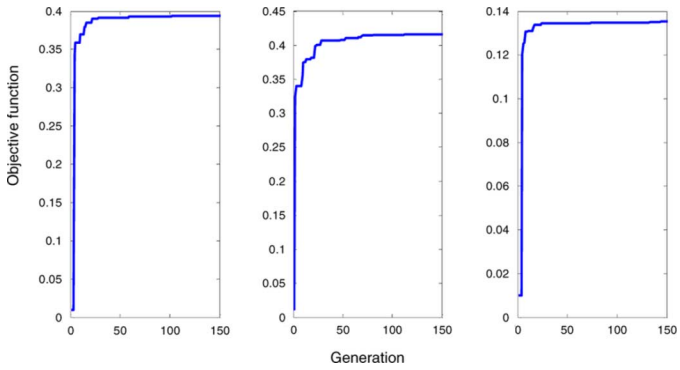

Fig. 11. Improvement of objective function.

A three-phase linear induction motor with aluminum sheet for handling materials application is chosen as the basis of design optimization. The minimum value of the efficiency and power in the algorithm is chosen close to their initial values of the nonoptimized motor. Therefore, we can be sure that neither the efficiency nor the power factor has been deteriorated. The genetic algorithm is then employed to search for optimal values of design variables. Three sets of the power coefficient are used to optimize the motor. In the first step, only the efficiency is optimized by using $k_1 = 1$ and $k_2 = 0$. In the second step, only the power factor is optimized using $k_1 = 0$ and $k_2 = 1$. Eventually, in the third step both the efficiency and power factor are optimized simultaneously using $k_1 = k_2 = 1$. The results of optimization are listed in Table III.

Fig. 11 shows the enhancement of objective function during different generations in these three optimizations steps.

V. FINITE-ELEMENT ANALYSIS

The design optimizations in this work were carried out based on the analytical model of the machine presented in Section II. Therefore, validity of the design optimizations greatly depends on the accuracy of the model. However, the model is obtained

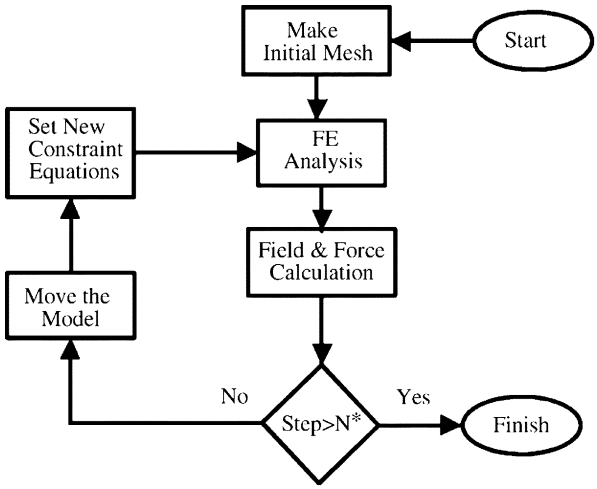

Fig. 12. Flowchart of FEA.

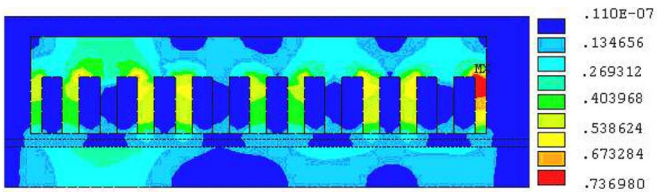

Fig. 13. Flux density distribution in the LIM.

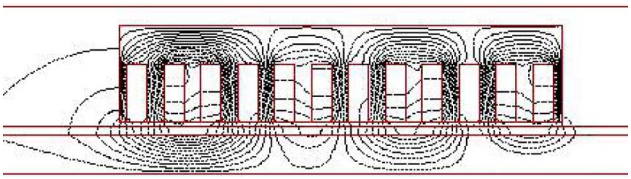

Fig. 14. Flux lines in the LIM.

by some simplifications such as ignoring end effect, saturation, nonlinearity of materials, etc. Thus, it is necessary to evaluate the extent of model accuracy. In this section, 2-D and 3-D time-stepping FEMs are employed to validate the model.

The fundamental equations of the magnetic field with eddy currents taken into account can be written as follows [22]:

$$\nabla \times (\upsilon \nabla \times A) = J_0 + J_e \tag{21}$$

$$J_e = -\sigma \left(\frac{\partial A}{\partial t} + \text{grad}\phi \right) \tag{22}$$

$$\nabla \cdot J_e = 0. \tag{23}$$

2-D FEM is carried out for the third optimal design and numerical and graphical results are obtained. The incomplete Cholesky conjugate gradient (ICCG) method is used to solve the finite-element equations. The relative movement is taken into account in the FEM by using time-stepping analysis and Lagrange multiplier method [23]. The forces are then calculated using local virtual work method. A flowchart of the FEM is shown in Fig. 12. The iron loss is also included in FEM. Figs. 13 and 14 show the flux density distribution and graphical representation of flux lines in the analyzed LIM, respectively.

TABLE IV
COMPARISON OF ANALYTICAL AND FEM RESULTS

Optimal Motor 1	Analytical	2D FEM	3D FEM
Efficiency	0.327	0.343	0.320
Power factor	0.415	0.385	0.384
Obj. Fun	0.135	0.134	0.122

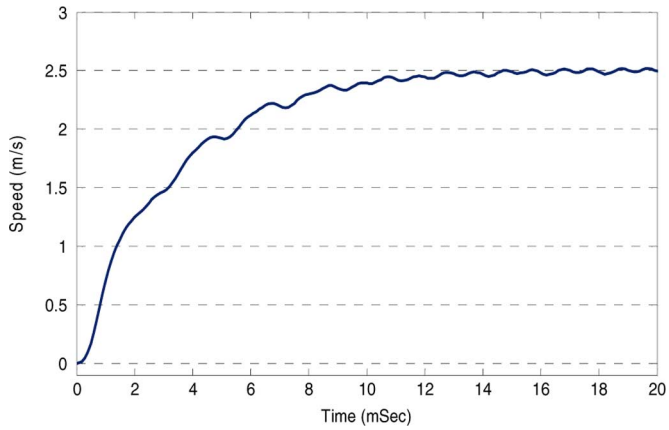

Fig. 15. Speed curve of the LIM at starting.

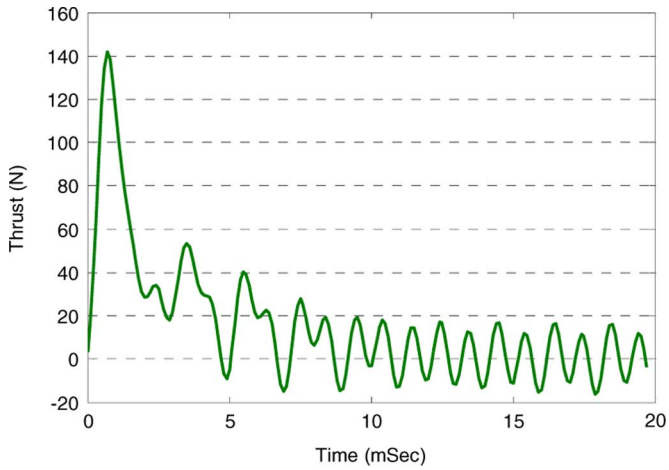

Fig. 16. Thrust curve of the LIM at starting.

It is seen that the flux lines are localized in front of the LIM and expand behind the LIM due to velocity effect.

The optimized design is simulated and its specifications are obtained by the FEM. Results of analytical method and FEM are compared in Table IV. It is seen that analytical results are close enough to FEM results. The speed curve and the starting thrust of the optimized LIM are shown in Figs. 15 and 16, respectively. It is seen that after 20 ms the speed of the LIM reaches a steady state. It is also seen that the starting thrust is in the acceptable range.

The 3-D FEM is employed to investigate the effect of overhang and edge effect. Since 3-D FEM is very complicated and time consuming, only a short span of time has been modeled in 3-D simulation. Using edge elements, the electric scalar potential in (22) can be ignored, and (23) can be eliminated. Although taking electric scalar potential into account leads to an increase

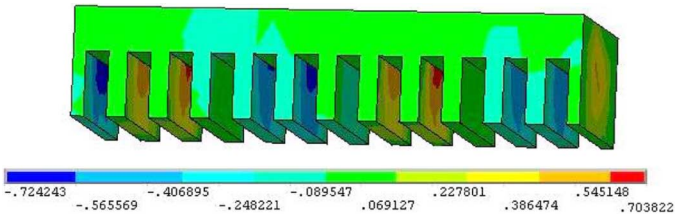

Fig. 17. Y component of flux density in the primary of the LIM.

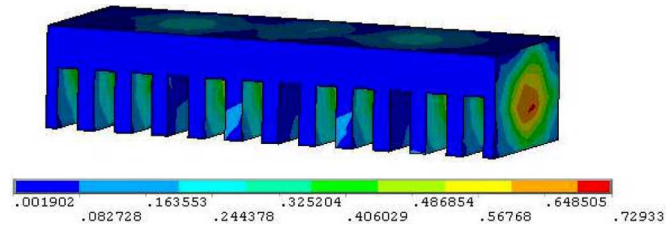

Fig. 18. Total flux density in the primary of the LIM.

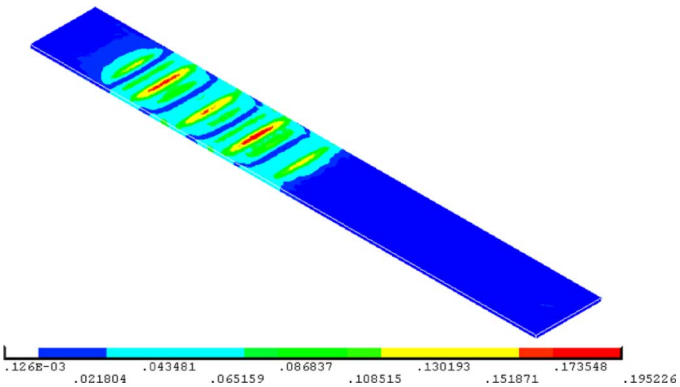

Fig. 19. Flux density distribution in the aluminum sheet.

in the number of unknown variables, it causes the reduction of ICCG iteration [24].

The normal component of the flux density and the total flux density in the primary of the analyzed LIM are shown in Figs. 17 and 18, respectively. Comparison of Fig. 15 with Fig. 18 shows that flux densities of primary in two models (2-D and 3-D) are close enough. The flux density distribution and the eddy-current distribution in the aluminum sheet are shown in Figs. 19 and 20, respectively. It is seen that the flux density of the aluminum sheet is around 0.2 T, which is close to the air gap flux density. The circular pass of the eddy current appears in Fig. 20. The loss due to current is calculated in the analysis. Therefore, the efficiency in this model is relatively lower than those in the analytical and 2-D FEM. The results obtained from 3-D FEM are listed in Table IV.

VI. Conclusion

A multiobjective optimization method was applied to a linear induction motor to improve both efficiency and power factor simultaneously. The analytical model based on magnetic equivalent circuit was used to calculate efficiency and power factor. The effect of different motor parameters on the efficiency and power factor were investigated through appropriate 2-D and 3-D

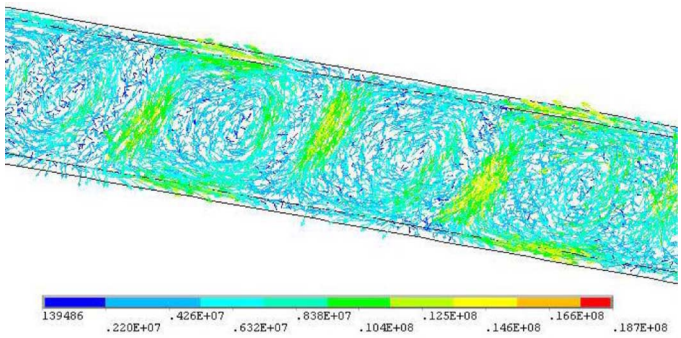

Fig. 20. Eddy-current distribution in the aluminum sheet.

plots. Motor parameters and dimensions were optimized using the genetic algorithm. It is seen that in the first and second optimization steps, the power factor increases up to 31% and the efficiency increase up to 9.2% separately. In the third optimization step, the product of the efficiency and the power factor rises about 12.5%. The results are then verified by 2-D and 3-D finite-element methods.

Appendix
List of Symbols

A	Magnetic vector potential.
a	Primary width.
a_e	Effective primary width.
B_{g1}	First harmonic of air gap flux density.
d	Al sheet thickness.
f_l	Primary frequency.
$g_{\rm ei}$	Modified air gap length.
g_m	Mechanical air gap.
I	Primary phase current.
J_m	Equivalent layer current density.
J_c	Primary winding current density.
J_e	Eddy-current density.
J_0	Source current density.
k_w	Primary winding factor.
$l_{\rm ce}$	End connect length.
m	Phase number.
$N_{\rm ph}$	Winding turn number.
p	Pole pairs number.
q	Slot per pole per phase.
R_1	Primary resistance.
R_2'	Secondary resistance referred into primary.
s	Slip.
V	Input voltage.
X_1	Primary inductance.
X_2'	Secondary inductance referred into primary.
μ_0	Air permeability.

υ	Reluctivity.
σ_{ei}	Modified aluminum conductivity.
σ_c	Cu conductivity.
τ	Pole pitch.
ϕ	Electric scalar potential.

ACKNOWLEDGMENT

This work was supported in part by the Center of Excellence on control and intelligent processing at the University of Tehran. The authors wish to thank the Center of Excellence on control and intelligent processing at the University of Tehran for supporting this research. The authors thank A. N. Khodabakhsh for his contribution in 3-D finite-element analysis.

REFERENCES

[1] J. F. Eastham, "Novel synchronous machines: Linear and disc," *Proc. Inst. Elect. Eng.*, vol. 137, pp. 49–58, Jan. 1990.

[2] J. F. Gieras, *Linear Induction Drives*. Oxford, U.K.: Oxford Univ. Press, 1994.

[3] I. Boldea and S. A. Nasar, *Linear Electromagnetic Device*. New York: Taylor & Francis, 2001.

[4] T. Koseki and S. Sone, "Investigation of secondary slot pitches of a cage-type linear induction motor," *IEEE Trans. Magn.*, vol. 29, no. 6, pp. 2944–2946, Nov. 1993.

[5] P. Blanc, T. T. Xuan, and R. Deshais, "Design calculations for annular induction electromagnetic pumps based on the finite element method," *IEEE Trans. Magn.*, vol. MAG-18, no. 2, pp. 650–654, Mar. 1982.

[6] T. C. O'Connell and P. T. Krein, "Development of a first-principles design method for electromechanical systems and a linear induction machine," in *Proc. Int. Electr. Machines Drives Conf.*, San Antonio, TX, 2005, pp. 474–480.

[7] S. Nonaka and S. T. Higuchi, "Elements of linear induction motor design for urban transit," *IEEE Trans. Magn.*, vol. MAG-23, no. 5, pp. 3002–3004, Sep. 1987.

[8] S. Osawa *et al.*, "Light-weight type linear induction motor and its characteristics," *IEEE Trans. Magn.*, vol. 28, no. 5, pp. 3003–3005, Sep. 1992.

[9] T. Yokoit and D. Ebzhara, "An optimal design technique for high speed mathematical programming method," *IEEE Trans. Magn.*, vol. 25, no. 5, pp. 3596–3598, Sep. 1989.

[10] S. Kikuchi, Y. Hashimoto, and R. Ebizuka, "Some considerations on the reduction of a noise in a LIM," *IEEE Trans. Magn.*, vol. 32, no. 5, pp. 5031–5033, Sep. 1996.

[11] M. Kitamura, N. Hino, H. Nihei, and M. Ito, "A direct search shape optimization based on complex expressions of 2-dimensional magnetic fields and forces," *IEEE Trans. Magn.*, vol. 34, no. 5, pp. 2845–2848, Sep. 1998.

[12] B. Laporte *et al.*, "An approach to optimize winding design in linear induction motors," *IEEE Trans. Magn.*, vol. 33, no. 2, pp. 1844–1847, Mar. 1997.

[13] T. Mishima, M. Hiraoka, and T. Nomura, "A study of the optimum stator winding arrangement of LIM in maglev systems," in *Proc. IEEE Int. Conf. Electr. Machines Drives, IEMDC*, 2005, pp. 1231–1242.

[14] T. Yokoi and D. Ebihara, "High-speed and high-thrust linear induction motor designed by using eigenvalue analysis method," *IEEE Trans. Magn.*, vol. 28, no. 5, pp. 3327–3329, Sep. 1992.

[15] D.-H. Im *et al.*, "Design of single-sided linear induction motor using the finite element method and SUMT," *IEEE Trans. Magn.*, vol. 29, no. 2, pp. 1762–1766, Mar. 1993.

[16] J. R. Wells *et al.*, "Linear induction machine design for instructional laboratory development," in *Proc. Electr. Insulation Conf. Electr. Manuf. Coil Winding Conf.*, Cincinnati, OH, 2001, pp. 319–322.

[17] B. K. Mukherjee, M. Sengupta, S. Das, and A. Sengupta, "Design, fabrication, testing and finite element analysis of a lab-scale LIM," in *Proc. IEEE Indian Annu. Conf.*, India, 2004, pp. 586–589.

[18] C. M. Neto, G. M. Jacinto, and C. B. Cabrita, "Optimised design aided by computer of single-sided, three-phase, linear induction actuators," in *MELECON '98. 9th Mediterranean Electrotechnical Conf. Proc.*, Tel-Aviv, Israel, 1998, vol. 2, pp. 1157–1160.

[19] S. B. Yoon *et al.*, "Analysis and optimal design of the slit type low speed linear induction motors," in *IEEE Int. Electr. Mach. Drives Conf.*, 1997, pp. TB2-8.1–TB2-8.3.

[20] S. Yoon, J. Hur, and D. Hyun, "A method of optimal design of single-sided linear induction motor for transit," *IEEE Trans. Magn.*, vol. 33, no. 5, pp. 4215–4217, Sep. 1997.

[21] D. E. Goldenberg, *Genetic Algorithms in Search, Optimization, and Machine Learning*. Reading, MA: Addison-Wesley, 1989.

[22] T. Yamaguchi, Y. Kawase, M. Yoshida, Y. Saito, and Y. Ohdachi, "3D finite element analysis of a linear induction motor," *IEEE Trans. Magn.*, vol. 37, no. 5, pp. 3668–3671, Sep. 2001.

[23] D. Rodger, H. C. Lai, and P. J. Leonard, "Coupled element for problems involving movement," *IEEE Trans. Magn.*, vol. 26, no. 2, pp. 548–550, Mar. 1990.

[24] K. Fujiwara, T. Nakata, and H. Ohashi, "Improvement of convergence characteristics of ICCG method for the A- φ method using edge elements," *IEEE Trans. Magn.*, vol. 32, no. 3, pp. 804–807, May 1996.

Manuscript received August 24, 2007; revised November 9, 2007. Corresponding author: B. M. Ebrahimi (e-mail: ebrahimibm@ut.ac.ir).

A. Hassanpour Isfahani (S'05) was born in Isfahan, Iran, in 1980. He received the B.Sc. degree in electrical engineering from Isfahan University of Technology, Isfahan, Iran, in 2002 and the M.Sc. degree (with honors) in electrical power engineering (electrical machines) from the University of Tehran, Tehran, Iran, in 2005, where he is working toward his Ph.D. degree now. His research interests include design, modeling, and control of electrical machines and finite element analysis of electromagnetic devices.

B. M. Ebrahimi was born in Kermanshah, Iran, in 1978. He received the B.Sc. degree in electrical engineering in 2002 and and the M.Sc. degree (with honors) in electrical power engineering (electrical machines) in 2006 from Tabriz University, Tabriz, Iran. He is now working toward the Ph.D. degree at the University of Tehran, Tehran, Iran. His research interests include design, modeling, control, and fault diagnosis of electrical machines and finite-element analysis of electromagnetic devices.

H. Lesani received the M.S. degree in electrical power engineering from the University of Tehran, Tehran, Iran, in 1975, and the Ph.D. degree in electrical engineering from the University of Dundee, U.K., in 1987.

Early in his career, he served as a Faculty Member with Mazandaran University. After obtaining the Ph.D. degree, he joined the Department of Electrical and Computer Engineering, Faulty of Engineering, University of Tehran, where he is an Associate Professor. His teaching and research interests are design and modeling of electrical machines and power systems.